FINAL PROJECT REPORT # 00042134-01-3A

GRANT: DTRT13-G-UTC45
Project Period: 6/1/2014 – 12/31/2019

Volume III:

Performance of Fiber-Reinforced Self-Consolidating Concrete for Repair of Bridge Sub-Structures and Fiber Reinforced Super Workable Concrete for Infrastructure Construction

Participating Consortium Member:
Rutgers, The State University of New Jersey

Authors:
Haider Abdulhameed
Graduate Research Assistant
Rutgers, The State University of New Jersey

Hani Nassif, PE, Ph.D.
Professor and Associate Director
Rutgers, The State University of New Jersey

Chaekuk Na, Ph.D.
Research Associate
Rutgers, The State University of New Jersey

RE-CAST:
REsearch on Concrete Applications for Sustainable Transportation
Tier 1 University Transportation Center

DISCLAIMER

The contents of this report reflect the views of the authors, who are responsible for the facts and the accuracy of the information presented herein. This document is disseminated under the sponsorship of the U.S. Department of Transportation's University Transportation Centers Program, in the interest of information exchange. The U.S. Government assumes no liability for the contents or use thereof.

TECHNICAL REPORT DOCUMENTATION PAGE

1. Report No. RECAST UTC # 00042134-01-3A	**2. Government Accession No.**	**3. Recipient's Catalog No.**
4. Title and Subtitle Volume III: Performance of Fiber-Reinforced Self-Consolidating Concrete for Repair of Bridge Sub-Structures and Fiber Reinforced Super Workable Concrete for Infrastructure Construction		**5. Report Date** January 2020 **6. Performing Organization Code:**
7. Author(s) Haider Abdulhameed, Hani Nassif, Chaekuk Na		**8. Performing Organization Report No.** Project # 00042134-01-3A
9. Performing Organization Name and Address RE-CAST – Missouri University of Science and Technology 500 W. 16th St., 223 ERL Rolla, MO 65409-0710		**10. Work Unit No.** **11. Contract or Grant No.** USDOT: DTRT13-G-UTC45
12. Sponsoring Agency Name and Address Office of the Assistant Secretary for Research and Technology U.S. Department of Transportation 1200 New Jersey Avenue, SE Washington, DC 20590		**13. Type of Report and Period Covered:** Final Report Period: 6/1/2014 – 12/31/2019 **14. Sponsoring Agency Code:**
15. Supplementary Notes The investigation was conducted in cooperation with the U. S. Department of Transportation.		
16. Abstract The main objectives of the project are: 1) Develop mix design(s) and examine fresh and hardened properties of SCC and FR-SCC mixes using two types of fibers and varying the proportion, 2) Investigate the compatibility and bond strength of FR-SCC as a repair material and select the mixes that yield the best performance and 3) Evaluate the structural performance of full-scale repaired beams that have corrosion and concrete cover spalling.		
17. Key Words Bridge substructures; Bridge superstructures; Fiber reinforced concrete; Infrastructure; Maintenance; Performance based specifications; Self describing data. Crack resistance, Expansive agent, Fiber reinforced concrete, Flexural behavior, Macro fibers, Micro fibers, Repair, Super workable concrete.	**18. Distribution Statement** No restrictions. This document is available to the public.	
19. Security Classification (of this report) Unclassified	**20. Security Classification (of this page)** Unclassified	**21. No of Pages** 32

Form DOT F 1700.7 (8-72) Reproduction of form and completed page is authorized.

Table of Contents

List of Figures

List of Tables

1. Introduction

1.1 Problem Statement

In the United States and worldwide, much of the existing infrastructure shows advanced stages of deterioration. Corrosion of steel reinforcement is the most common type of failure for concrete bridges due to chemical attack by acids, sulfates, and even soft water. Another type of failure occurs when concrete constituents absorb water and react, which usually leads to disintegration or expansion [Newman and Choo, 2003].

An appropriate maintenance schedule is key to extending the service life of the infrastructure. The cost of repair, strengthening, and protection of concrete structures in the Unites States was estimated to be $18 to $20 billion [Emmons, 2006]. It was also estimated in 2005 by the American Society of Civil Engineers (ASCE) report that $1.6 trillion would be needed to restore the deficient infrastructure in the US for the next five years [Goodwin, 2008]. The efficiency of the repairs depends on the repair material quality, repair method, and the compatibility/bond between the repair material and the substrate. One important aspect of bridge repair is the ability to fill in the congested reinforcement areas with fresh concrete.

Self-Consolidating Concrete (SCC) has been utilized for field application and is preferred over conventional concrete for the rehabilitation and repair of reinforced concrete structures. The conventional concrete is usually difficult to consolidate, and in some cases, vibration is not feasible. From this point of view, the self-compacting ability of SCC may have considerable advantages for bridge repair when compared to conventional concrete. At the same time, SCC can be designed to provide the desired hardened concrete properties for any field application, similar to conventional concrete or even high performance concrete (HPC). However, the SCC is highly prone to shrinkage because of its higher paste content compared to the conventional concrete. It has been suggested that using various types of fibers in SCC mixes, so-called Fiber Reinforced SCC (FR-SCC) could enhance the concrete's tensile strength and ductility, and could also delay the onset of tension cracks. However, the performance of such FR-SCC has not been fully evaluated for use as a repair material. Earlier studies and available literature indicate that the failure of concrete repair is mainly due to improper selection of repair material without investigating its compatibility with the substrate concrete. Thus, it is important to study the compatibility and bond performance between two different materials, and then evaluate the feasibility of FR-SCC for field application.

1.2 Literature Search

Since it's advent in 1986 at the Ouchi University of Technology in Japan, the self-consolidating concrete (SCC) has been extremely popular in construction due to its ability to consolidate by its own weight [Nawy, 2008]. Field repair implementation of SCC was performed at a parking garage in Quebec, in 1996 [Khayat et al, 1998]. The SCC was used to repair the underneath and sides of a 20-foot long beam that had substantial corrosion damage surrounding the joint at the entrance of the lot. Two 4" holes were bored through the upper deck of the beam along the outer length of the beam between the present substrate and formwork. The SCC successfully flowed and placed into the formwork despite the reinforcement obstacles.

The Quebec Department of Transportation's primary performance specifications for SCC in 1997 have been used in many repair projects. The enhanced performances of SCC have caught the attention of several other construction companies and transportation firms in both Canada and the United States. Figure 1 show examples of such repair efforts using SCC [Khayat et al. 2010, Ozyildirim, 2013].

Figure 1 – Application of SCC for Repair; (a) Bridge Pier Caps and Columns in Quebec [Khayat et al, 2010], (b) Pile Damaged by a Barge in Virginia [Ozyildirim, 2013], and (c) Damaged Column and Pier Cap in Virginia [Ozyildirim, 2013].

Concrete, especially cement-rich concrete like SCC is susceptible to cracking as a result of shrinkage. To mitigate the shrinkage cracking, fibers have been increasingly used to improve its tensile and flexural strength and cracking resistance. The use of fiber in the SCC matrix (FR-SCC) changes the crack formation and propagation mechanism significantly by the bridging effect or tension softening behavior, and therefore, the SCC with fibers will sustain more load after the formation of the first crack and multiple cracks will be formed [Vandewalle, 2002]. The benefits of using FRSCC as a repair material were exemplified in 2003 during the repair of the 860 ft Jarry/Querbes Underpass as shown in Figure 2. Due to repeated exposure to frost, the underpass experienced harsh deterioration. Of the 32 panels cast for the retaining walls, 29 were cast with FR-SCC. After completion of repair, the underpass was both visually pleasing and effectively repaired, with no cracking due to shrinkage. Because synthetic fibers were used to reinforce the repair concrete, the fresh repair was able to effectively fill voids while maintaining designed strength.

(a) (b) (c)

Figure 2 – Application of FR-SCC in Jarry/Querbes Underpass in Montreal [Khayat et al, 2005].

The performance of FR-SCC for repair of RC beams was studied to evaluate the influence of different types of fibers on the flexural response and durability for repair applications [Kassimi et al. 2014]. Two synthetics, one steel fiber, and one hybrid fiber with up to 0.5% by volume were used to repair beams, and ten repaired beams were tested under four-point bending over a simply supported span. The results showed that the use of optimized FR-SCC mixtures could replace 50% of reinforcement in repair sections of tension zone without mitigating structural performance, i.e., the number of bars was decreased from three bars to two bars.

1.3 Research Objectives

The main objectives of this project are summarized below:

- Develop mix design(s) and examine fresh and hardened properties of SCC and FR-SCC mixes using two types of fibers, and varying the proportion.

- Investigate the compatibility and bond strength of FR-SCC as a repair material and select the mixes that yield the best performance.

- Evaluate the structural performance of full-scale repaired beams that have corrosion and concrete cover spalling.

1.4 Research Methodology

The experimental program is designed to evaluate the performance of FR-SCC for use in repairing damaged concrete structures. The work is divided into three phases;

Phase 1: Develop the SCC and FR-SCC mix designs for structural repair. Based on various trial mixes, the optimized mix designs that provide the best fresh and hardened mechanical properties will be selected.

Phase 2: Perform compatibility and bond strength tests for the mixes selected in Phase 1.

Phase 3: Study the flexural behavior of full-scale repaired beams to evaluate the structural performance of the repair. Corrosion damage and concrete spalling are simulated by the smaller rebar diameter.

2. Laboratory Testing Program

2.1 Phase 1 – Development of SCC and FR-SCC Mix Designs

2.1.1 Mix Design and Materials

The first phase of the experimental program was conducted to develop the mix designs and obtain the fresh and hardened concrete properties of SCC and FR-SCC mixes. A control mix (Portland cement only SCC), and twelve (12) SCC mixes with two types of Pozzolanic admixtures (Silica Fume (SF) and Slag Grade 120 (SL)) were prepared. In addition to these, steel fibers (STF) and polypropylene fibers (PPF) with various volume contents were prepared for SCC mixes with Pozzolans to select the best mix designs that satisfy various requirements. Table 1 shows the matrix of mixes and their abbreviations, as well as the control mix design.

Materials were obtained from different local NJ suppliers. Fine and coarse aggregates were obtained from Clayton Concrete plant in Edison, NJ. Type I Portland Cement was provided by Buzzi Unicem in Stockertown PA, and Grade 120 Slag was supplied by LaFargeHolcim in Bayonne, NJ. Chemical admixtures, and the steel and polypropylene fibers were provided by Euclid Chemical in East Brunswick, NJ. The supplier for each material is summarized in Table 2. All materials comply with ASTM standards.

The steel fiber (STF) is a crimped macro fiber with a length of 1.5 in. known commercially as PSI Crimped Steel Fiber. The aspect ratio of STF is 34 and the tensile strength is between 140-180 ksi. The polypropylene fiber (PPF) is a micro fiber with a length of 1/4 in. known commercially as PSI Fiberstrand 100. The specific gravity of PPF is 0.91 and the denier is 15. Detailed technical specifications can be found on the supplier's webpage at http://www.euclidchemical.com. Figure 3 shows both types of fibers used in this study.

Table 1 – Mix Proportions

Mix/ Abbreviation	Silica Fume replacement (SF)	Slag replacement (SL)	Steel Fiber, STF (S)	Polypropylene Fiber, PPF (P)
Control	Type I Cement=675 lbs. (w/c=0. 425), #8 and sand=1436 lbs.			
10SF	10%	-	-	-
10SF25S	10%	-	0.25%	-
10SF50S	10%	-	0.50%	-
10SF10P	10%	-	-	0.10%
10SF15P	10%	-	-	0.15%
10SF20P	10%	-	-	0.20%
35SL	-	35%	-	-
35SL25S	-	35%	0.25%	-
35SL50S	-	35%	0.50%	-
35SL15P	-	35%	-	0.15%
35SL20P	-	35%	-	0.20%
35SL25P	-	35%	-	0.25%

Table 2 – Materials and suppliers

Material	Type	Supplier
Cement	Portland Type I	Buzzi Unicem
GGBFS (Slag)	Grade 120	LaFargeHolcim
Fine Aggregate	Concrete Sand	Clayton Concrete
Coarse Aggregate	#8 (3/8") granite	Clayton Concrete
Polypropylene Fiber	PSI Crimped	Euclid Chemical
Steel Fiber	PSI Fiberstrand 100	Euclid Chemical
HRWR	Plastol 5000	Euclid Chemical

(a) Steel Fiber (STF) (b) Polypropylene Fiber (PPF)

Figure 3 – Two Types of Fiber

2.1.2 Fresh Concrete Property Testing

Four different tests for fresh concrete properties were performed as shown in Figure 4. The Slump Flow test was conducted in accordance with ASTM C1611. A sample of fresh concrete was placed in inside of an inverted slump cone. The concrete was placed in one layer without tamping or vibration, and then the cone was lifted. After the concrete spread, the diameter was measured twice in orthogonal directions, and the average of the two diameters is the Slump Flow. The J-ring test was performed according to ASTM C1621. The procedure is the same as in the Slump Flow test, but it requires an additional ring with 16 vertical rebars. The difference between the Slump Flow and J-Ring Flow is an indicator of the passing-ability of the concrete. A modified L-box Test with one rebar instead of three was used to measure the filling-ability of FR-SCC, and the modification was made to compensate for the slow flow reduction due to the use of fibers. The filling-ability of the L-box test is described by the ratio of the concrete height at the end of the horizontal section (h2) to the height at the beginning of the horizontal section (h1). When a visual inspection of the horizontal section and the area around the rebar shows an even distribution of aggregate, the mix has a good filling-ability. The air content test was carried out in accordance with ASTM C231 using a Type-B pressure meter.

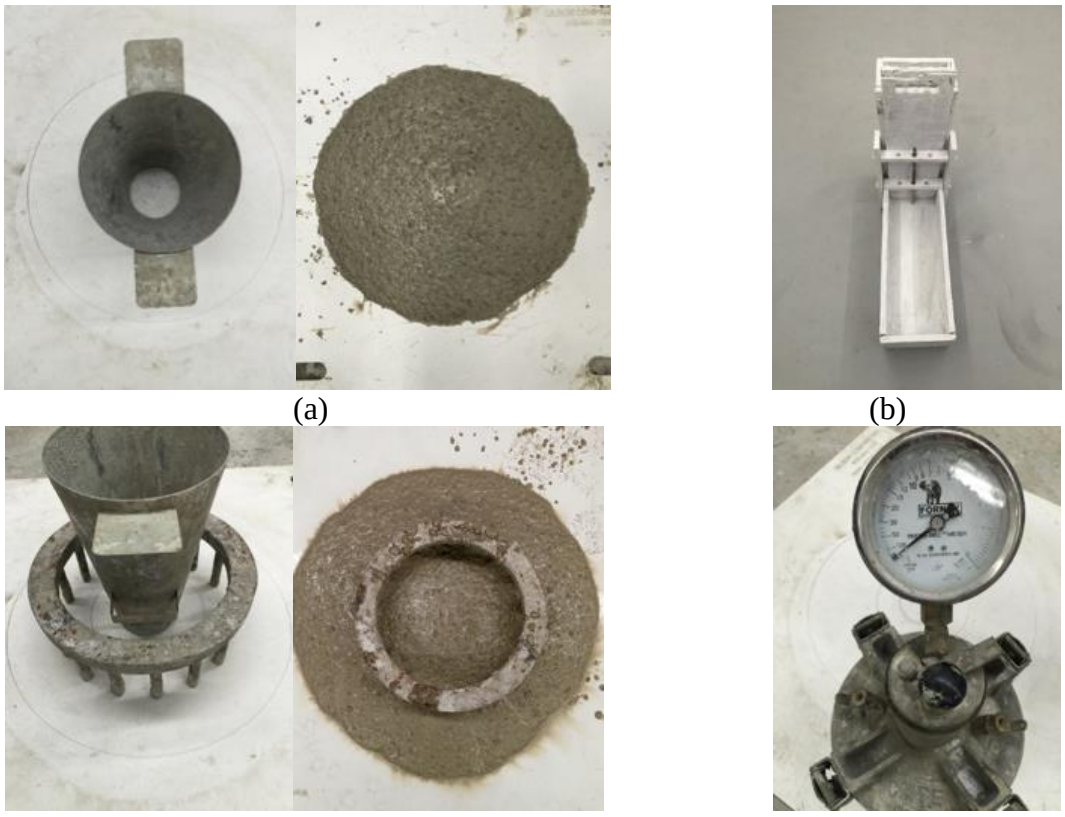

(a) (b) (c) (d)

Figure 4 – Fresh Concrete Test; (a) Slump Flow Test, (b) L-Box Test, (c) J-Ring Test, and (d) Air Chamber

2.1.3 Hardened Concrete Property Testing

The compressive strength, splitting tensile strength, and modulus of elasticity tests were performed in accordance with ASTM C 39, C 496 and C 469, respectively, using 4 × 8-in. cylinders. The flexural testing was carried out on 4 × 4 × 16-in. prism specimens in accordance with ASTM C 78.

Compressive Strength Test

The compressive strength test was performed in accordance with ASTM C 39, using 4 × 8-in. cylinders. The compressive strength of the cylinders was tested using a standard testing machine with a capacity of 1 Million pounds as shown in Figure 5 (a). The specimen was loaded at a rate of 4000 lbs. every 9 seconds, and Figure 5(b) shows an example of testing cylinder. The average of the three specimens was recorded for each testing age.

Modulus of Elasticity Test

The static modulus of elasticity was conducted on 4 × 8-in. cylinder specimens in accordance with ASTM C 469 using the same compression machine used for the compressive strength test. Figure 5 shows the test setup with a cage and dial gauge to measure the displacement while load is being applied. The load was first applied at 35~40% of its compressive strength without any measurement, and then two consecutive tests were performed to measure the displacement at every 4000 lb. of loading.

(a) (b) (c)

Figure 5 – Compressive Strength and Modulus of Elasticity Test; (a) Compressor Machine, (b) Compressive Strength Test, and (c) Modulus of Elasticity Test

Splitting Tensile Strength Test

The splitting tensile strength test was performed in accordance with ASTM C 496. 4 × 8-in cylinders were tested on a standard compression machine at a rate of 100 lbs. per second. Figure 6(a) shows the test setup with one plywood strip placed on the top, and one on the bottom of the curved cylinder side to distribute the load evenly. The average strength of three cylinders was taken at each testing age.

Flexural Strength Test

This test was carried out on 4 × 4 × 16-in. specimens in accordance with ASTM C78 using an MTS flexural strength testing machine. Figure 6(b) shows the test setup. The theoretical maximum tensile stress reached in the bottom fiber of the test beam is known as the modulus of rupture.

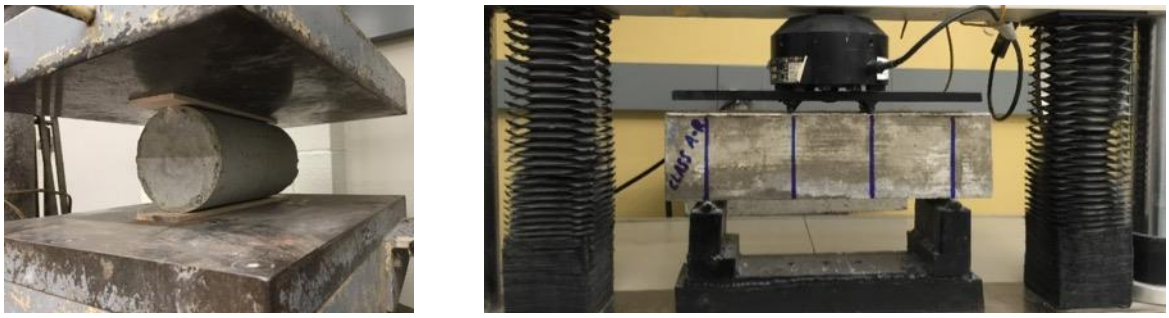

(a) (b)

Figure 6 – (a) Tensile Strength and (b) Flexural Strength Test

The free shrinkage test was performed in accordance with ASTM C157. The specimens were 3 × 3 × 11 in. prisms with an embedded stud at each end. Immediately after the shrinkage specimens were prepared, they were covered with a plastic sheet to avoid any moisture loss, and then cured in the curing room for 14 days. Then samples were moved to an environmental chamber with a controlled ambient temperature of 74°F and relative humidity of 50% for 6 months.

2.2 Phase 2 – Compatibility and Bond Strength of FR-SCC

The second phase was performed to investigate the compatibility and bond strength of FR-SCC mixes with the substrate concrete. The FR-SCC mix designs are taken from the Phase 1 study. The substrate concrete is Class A concrete to simulate the existing concrete properties and the mix design is summarized in Table 3. First, the specimens were partially cast using Class A concrete and cured for 28 days. In addition, some Class A concrete cylinders were fully cast for strength testing of the substrate, and the testing results are summarized in Table 4. The remaining part of half-filled Class A cylinder was filled by FR-SCC, and then the specimens were tested at 1, 3, and 28 days.

Table 3 – Mix Design for the Substrate (Class A)

Material	Mix Design (per CY)	Detail
Cement (lbs)	611	Essroc, Type I PC
Sand (lbs)	1275	Concrete sand, Clayton, NJ
Stone (lbs)	1800	#57, Weldon Quarry, NJ
Water (gal)	31	Tap Water
W/C	0.42	-
AEA (ozs)	4.9	Setcon 6A, Great Eastern Technologies, NJ
MRWR (ozs)	24.4	Polystrong HP, Great Eastern Technologies, NJ
Retarder (ozs)	12.2-30.6	Chestrong R, Great Eastern Technologies, NJ
Slump (in)	5-7	-
Air (%)	6 +/- 1.5	-

Table 4 – Substrate Strength Testing Results (Class A)

Age	1 day	3 days	28 days
Compressive Strength (psi)	3718	4498	5653
Splitting Tensile Strength (psi)	362	434	459
Modulus of Rupture (psi)	334	411	603
Modulus of Elasticity (ksi)	4121	4276	4591

2.2.1 Third Point Loading Test for Composite Beam

The composite beam was fabricated to evaluate compatibility of the repair material with substrate Class A concrete compared to the control beam without repair. Figure 7(a) illustrates the dimension of composite beam. The specimen size is 16 in. long and the cross-section is 4 in x 4 in. The composite beam has a wide-mouthed notch that is 4 in. long × 4 in. wide × 0.8 in. thick. The control and composite beams were moist cured for 28 days, and then the notched areas were textured using a steel brush to remove any abnormal surface particles. After the 7 day air-drying period, the notched area was cast and cured for additional 28 days. The composite beams were tested in a set up for the third point loading test in accordance with ASTM C78 as shown in Figure 7(b).

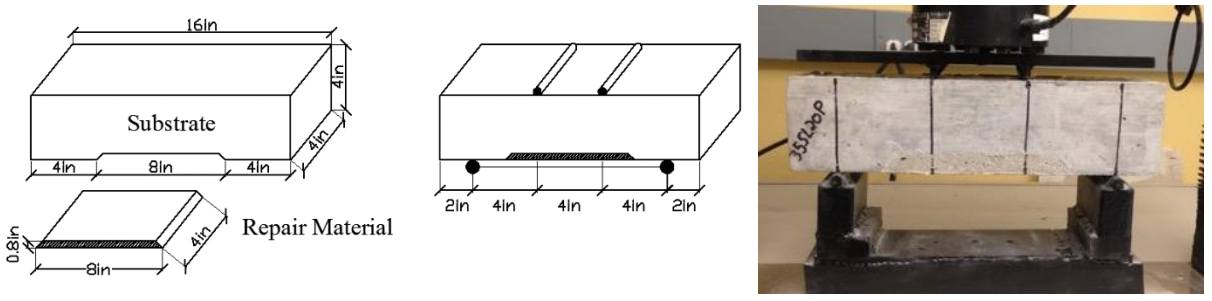

(a) Dimension (b) Third Point Loading Test

Figure 7 – Control and Composite Beam with Substrate

2.2.2 Bond Strength Test for Slanted Cylinder

The bond strength of the different repair materials was determined in accordance with ASTM C882 as shown in Figure 8(b). The repair material was bonded to the substrate concrete specimen on a slanted elliptical plane inclined at 30° from the vertical to form a 3 in. x 6 in. composite cylinder in Figure 8(a). A full 3 in. x 6 in. cylinder was casted and cured for 28 days, then cut using a concrete saw. The slanted surface of substrate concrete was cleaned and dried, and then FR-SCC was cast in the remaining portion of cylinder. The bond strength test was performed after 28 days of wet-curing as explained previously. The compressive load required to fail the composite cylinder was determined and the bond strength was calculated as the maximum applied load divided by the area of slanted surface.

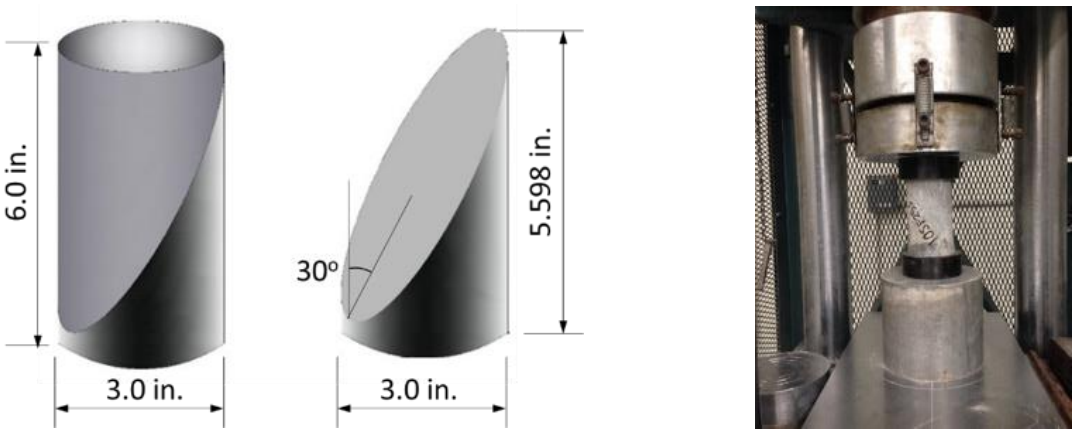

(a) Dimension (b) Bond Strength Test

Figure 8 – Slanted Cylinder with Substrate

2.3 Phase 3 – Full Scale Beam Testing

The last phase of this research is to cast ten (10) full-scale beams to study the flexural behavior and capacity of the FR-SCC repaired beam. There are two control beam specimens (one for Slag and the other for Silica Fume), while other 8 specimens have Class A substrate and FR-SCC repaired layer with smaller diameter of rebar.

2.3.1 Preparing and Casting Substrate

Ten wooden formworks and steel cages were prepared (Figure 9(a)). The formworks were 8-in wide, 12-in high and 12-ft long, and made using 3/4-in thick plywood. The formworks were coated with 3 layers of polyurethane as a repellent against the water from fresh concrete. The steel cages were constructed with #2 rebar for top reinforcement, #3 for stirrups, and either #3, #4 or #5 for bottom reinforcement. Figure 10 depicts the cross-sectional dimension of 10 beams. Different bottom reinforcements were used in order to simulate the damaged rebar by corrosion by 35% (#4) and 65% (#3) compared to #5 rebar.

A number of strain gauges were installed as per manufacturer procedure on the steel reinforcement to monitor the stain development during the flexural testing (Figure 9(b)). When the substrate was prepared with Class A, duct tape was applied on the bottom reinforcements (top reinforcement while casting, since the formworks were placed reversely) and shear stirrups to keep the reinforcements clean for the repair process.

The two control beams and 8 substrate beams were cast using Class A concrete mix provided by a local concrete supplier as shown in Figure 9(c). External vibrators were used to consolidate the concrete followed by spaying a retarding admixture on the concrete surface to delay the final setting of the substrate. The beams were covered with a plastic sheet until the next day (see Figure 9(d)) and the surface debris and duct tapes were removed and cleaned. The beams were wet-cured for 7 days and then air-cured until the day of repair.

(a) Formworks and steel cages

(b) Strain gauge installation

(c) Casting beams with conctere truck

(d) Curing beams

Figure 9 – Substrate Preparation

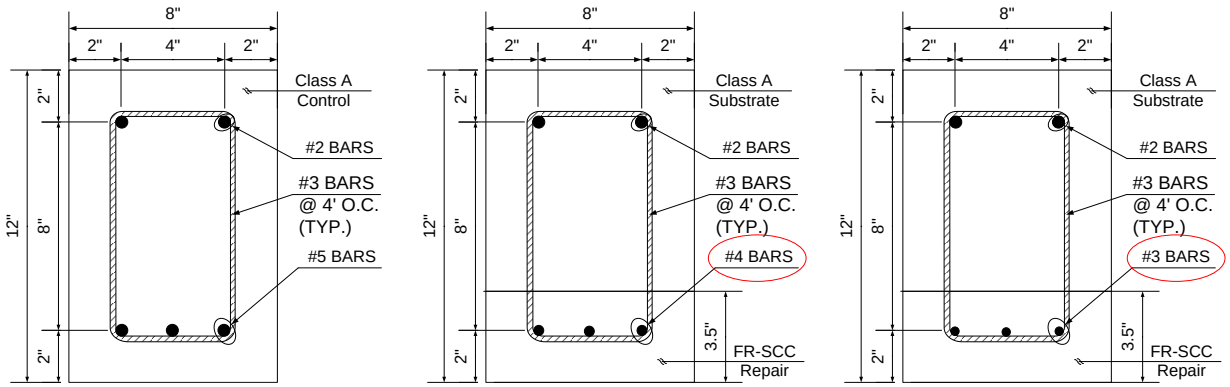

Control 1 / 2

10SF25S, 10SF10P
35SL25S, 35SL15P

10SF50S, 10SF15P
35SL50S, 35SL20P

Figure 10 – Cross Sectional Dimension

2.3.2 Repairing and Curing

The exposed reinforcements were cleaned from any rust and debris before repairing beams as illustrated in Figure 11(a). The substrate surface was also cleaned from any debris and wet to obtain a saturated surface. Each FR-SCC batch described in Phase 1 was prepared to repair the beam, and then the beam was covered with a wet-burlap and plastic sheet for 24 hours. On the next day, the beam was placed on a loading machine, and the surface was whitewashed divided into grids as shown in Figure 11(b). The testing instrumentation was prepared and the beam was tested at an age of 3 days after the beam repair was completed.

(a) Cleaned reinforcement before repair

(b) Painting beams for flexural testing

Figure 11 – Repairing Preparation

2.3.3 Beam Flexural Test Setup

Various types of sensors, such as foil strain gauge (FSG), vibrating wire strain gauge (VWSG) and linear variable differential transformer (LVDT), were instrumented at different locations to record the structural behavior. Figure 12 illustrates the test setup and instrument locations, and detailed information is summarized as follows:

- One LVDT (L1) was placed on the top surface at mid-span of the beam horizontally to measure the concrete compressive strain.
- Two LVDTs (L2) were placed horizontally at the expected crack locations. These LVDTs are high-accuracy with linearity error within ±0.5% based on full scale. The location is designed to monitor the crack width of the major cracks under the loading points.
- Two LVDTs (L3) were installed vertically at mid-span to monitor the maximum deflection during testing. Two sensors were used for redundancy.
- Two LVDTs (L4) were placed vertically at one-third and two-third of span (under the loading points) to control the deflection profile along the beam for quality control.
- One LVDT and one VWSG (LV) were installed at the interface between substrate and FR-SCC near the support to monitor a possible de-bond and delamination between two layers.
- Three foil strain gauges (FSGs) were pre-installed at each F1, F2 and F3 locations, and 2 FSGs were attached on the concrete surface at mid-span (See C1 and C2).
- Two FSGs (F1) were designed to monitor the strain developed on the shear stirrup.
- Two FSGs (F2) were glued to the longitudinal tensile reinforcing bars at third-span under the point loading to measure the tensile strain.
- Two FSGs (F3) were instrumented to measure the maximum strain development on the main reinforcement.
- Two FSGs (C1 and C2) were glued to different depths of the concrete beam at mid-span for quality control.

Figure 13 shows the LVDT, FSG and VWSG installed on the beam. Figure 13(a) shows the L2 location with one LVDT, Figure 13(b) shows two FSGs at C1 and C2 locations that were attached on the concrete surface, and Figure 13(c) shows the LV locations with one LVDT and one VWSG at the interface between two materials. Figure 13(d) shows the LVDTs at L3 and L4 locations, and Figure 13(e) shows the LVDT installed on the top of the beam.

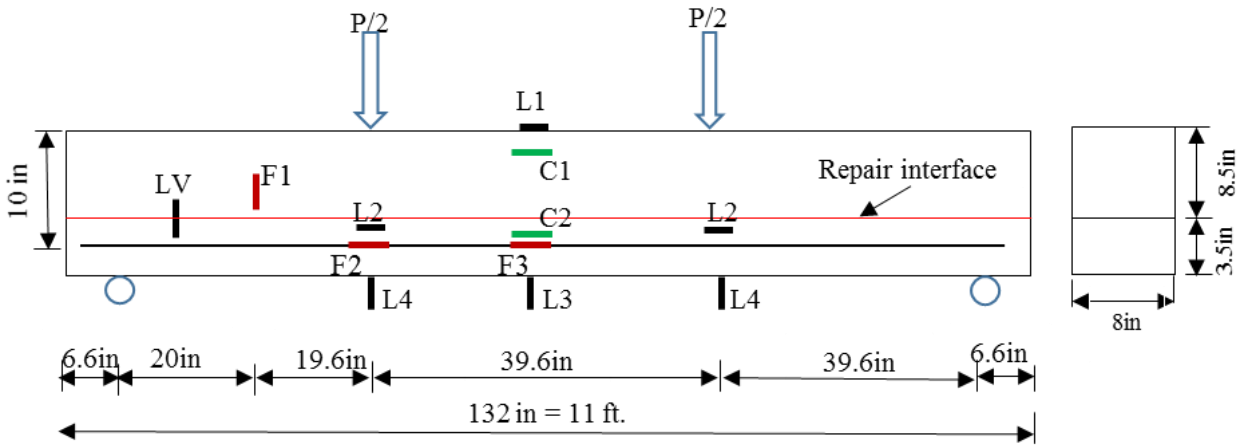

Figure 12 – Test Setup and Instrument Locations

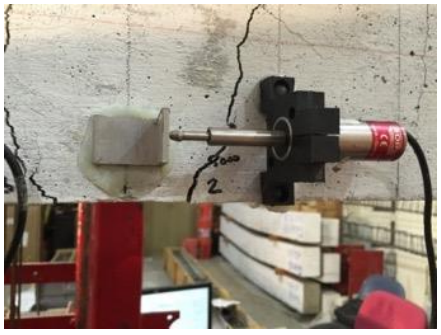

(a) LVDT (L2)

(b) FSG (C1 and C2)

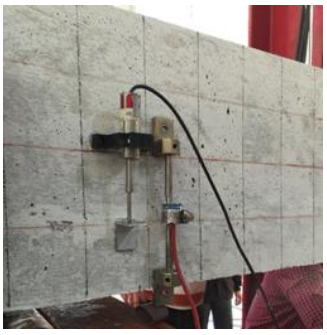

(c) LVDT and VWSG (LV)

(d) LVDT (L3 and L4)

(e) LVDT (L1)

Figure 13 – Sensor Instrumentation Setup

3. Concrete Performance Evaluation

3.1 Phase 1 Testing Results

3.1.1 Fresh Properties

Table 5 summarizes the fresh concrete properties of mixes described in Phase 1. The dosage of HRWR was adjusted to reach the target slump between 21.5 in. and 25.5 in. Additional dosage of HRWR was used for FR-SCC mixes to offset the reduction of slump flow due to the addition of fibers. Once the slump flow was achieved, the subsequent fresh concrete properties were measured. The results show that the effect of STF on slump flow is minimal while that of PPF is predominant. When the PPF volume exceeded 0.15% or 0.25% volume (see grey color in Table 5), the slump flow did not reach the target slump flow although the dosage of HRWR exceeded the upper limit of manufacturer recommendation.

Table 5 – Fresh Concrete Properties

Mix ID	HRWR (oz/cwt)	Slump Flow (in)	J-Ring (in)	T20 (sec)	L Box h2/h1	VSI	Air Content
Control 1	7	22.5×22	23×24	4	1	0	7%
Control 2	8.5	25×25	21.5×21	5	1	0	6.5%
35SL25S	7.5	21.5×19	20.5×19.5	5.5	1	1	6.5%
35SL50S	8.5	22×22	18.5×19	6.5	0.9	1	6.5%
35SL15P	10	23.5×23	19×16	4.5	0.9	0	6.5%
35SL20P	11	23×23	18×17	4.5	0.8	0	6%
35SL25P	32.9	18×16*	17×15	11	N/A	0	5.5%
10SF25S	12.3	25×22	21×21	5.3	0.95	0	6.5%
10SF50S	22	24×22	19×19	6	0.93	0	6%
10SF10P	17.2	23×20.5	18×17	5	0.9	0	6.5%
10SF15P	26.5	20×19*	17×17	8	0.8	0	6%

* Not qualified FR-SCC mix.

3.1.2 Mechanical Properties

Mechanical properties including compressive strength, splitting tensile strength, flexural strength, and modulus of elasticity were tested for the FR-SCC mixes at 1, 3 and 28 days after mixing. The samples were stored in the environmental chamber to provide steady temperature of 74^{o}F and relative humidity of 50%.

A total of 9 cylindrical samples from each mix were used for the mechanical testing. Six samples were capped using a sulfur capping compound to distribute the stress on the cylinder where three of which were for the compression test and other three were used for the modulus of elasticity test. The last 3 samples were used for the splitting tensile strength test. The cracking strain which is the splitting tensile strength divided by the modulus of elasticity, was also calculated. The cracking strain represents the cracking capacity that a mix can sustain before cracking begins.

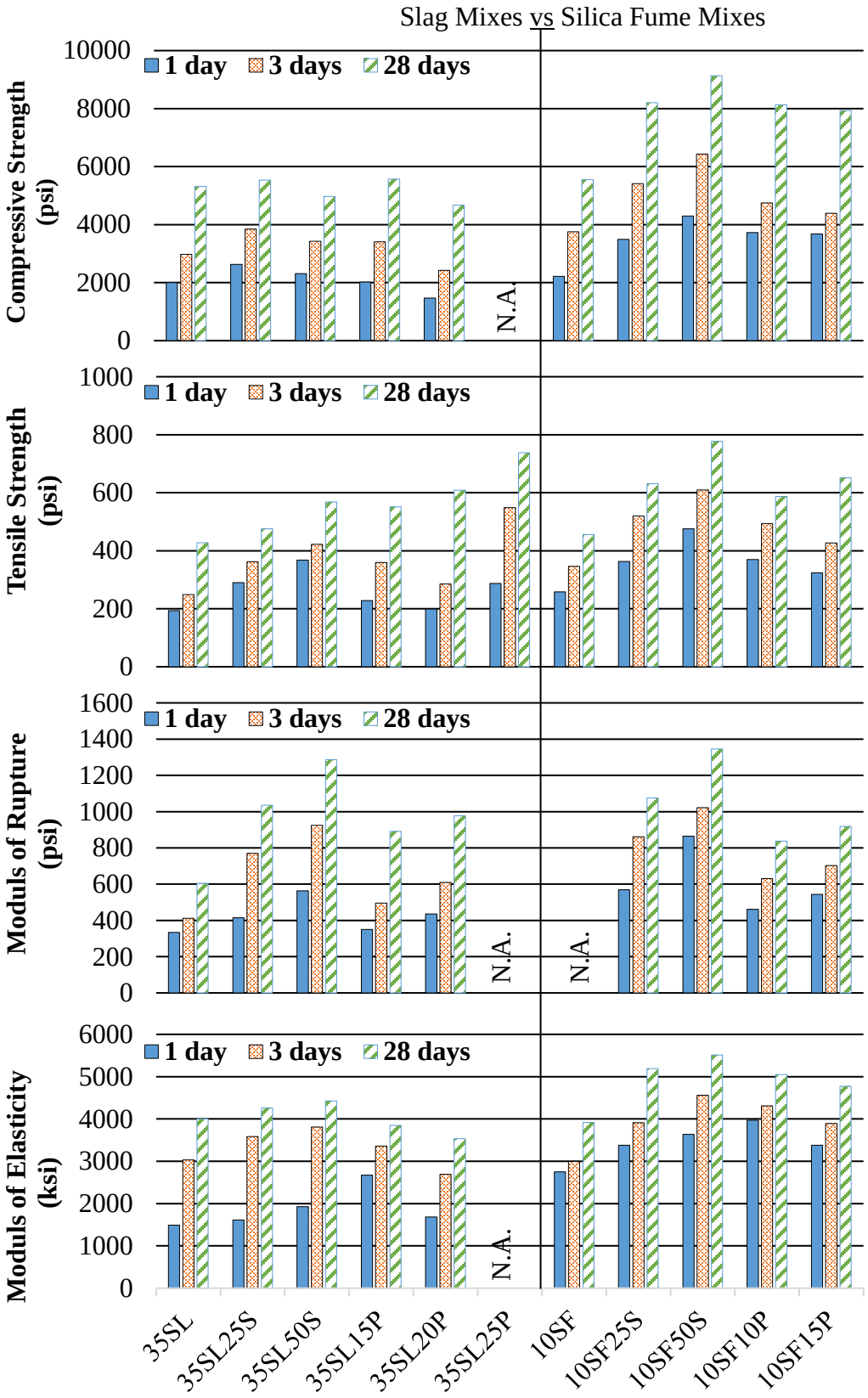

Figure 14 – Mechanical Testing Results

Six prism specimens were prepared and two per each age were tested to measure the modulus of rupture at 1, 3, and 28 days after mixing. Two-point load was applied at one- and two-third of the beam, and the maximum applied load was recorded.

Figure 14 represents the mechanical strength development at various ages for all mixes listed in Phase 1. Results show that SF mixes obtained comparatively higher compressive strength compared to SL mixes, and the increase of fiber content slightly reduced the compressive strength. The increase in compressive strength of SF mixes was because the fineness of silica fume is higher and therefore silica fume is more reactive than slag. The addition of steel fibers to concrete increased the splitting tensile strength of concrete significantly. This behavior is attributed to the mechanism of steel fibers in arresting crack propagation. The modulus of rupture increased with the increase of fiber percentage. This behavior is mainly attributed to the role of steel fibers in releasing fracture energy around crack tips which is required to extent crack growing by transferring it from one side to another side. The modulus of elasticity was also increased by the addition of fiber content.

Figure 15 illustrates the free shrinkage test results of 11 mixes. SF mixes obtained higher shrinkage strain compared to SL mixes probably because SF is more active than SL. The results show that the incorporation of both fibers reduced the shrinkage significantly comparing to control mix without fiber. It is worth to mention that 35SL50S mix showed the lowest shrinkage and it reduced the shrinkage by 37 % compared to control mix (35SL) at 56 days.

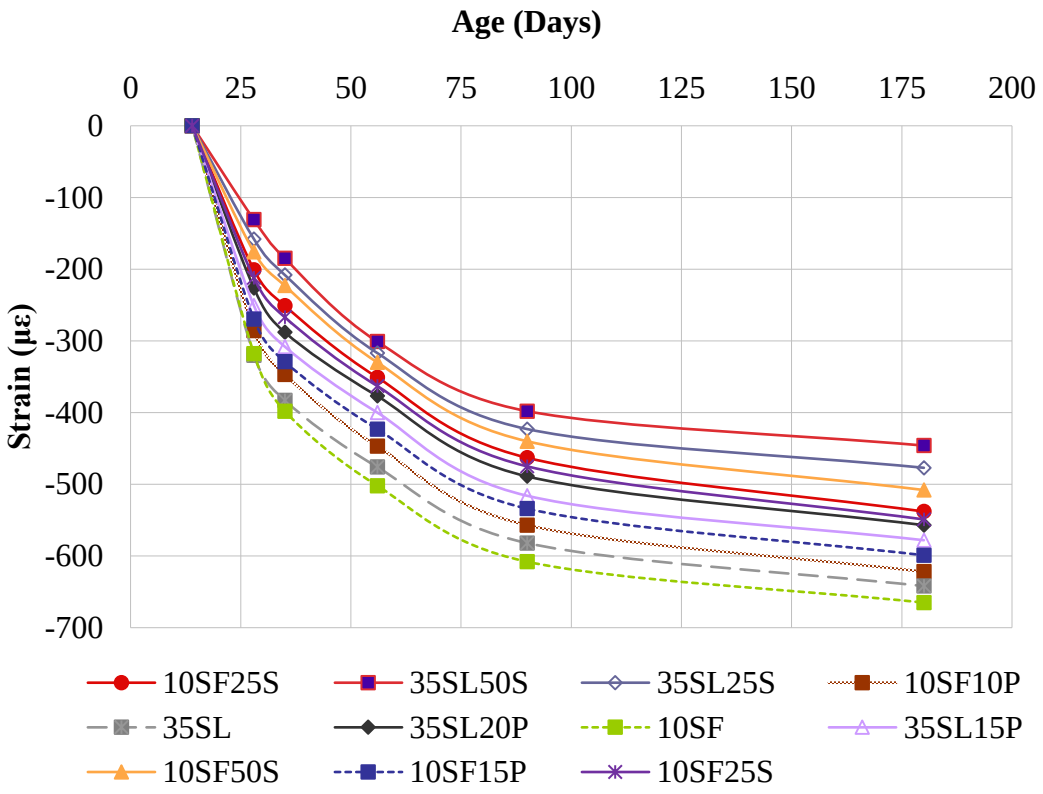

Figure 15 – Shrinkage Testing Results

3.2 Phase 2 Testing Results

3.2.1 Compatibility Test (Flexural Strength)

The flexural strength or compatibility testing results are presented in Figure 16. The top figure shows the flexural strength of FR-SCC beams (no repair and no substrate), while the bottom figure illustrates the flexural strength of composite beams with Class A substrate and FR-SCC repair. Figure 17 represents the correlation between the flexural strength of the FR-SCC beam and that of the composite beam with corresponding FR-SCC. For all cases, the failure location was the mid-point which indicates a good compatibility between two distinct materials. The results show that higher fiber content increased the flexure strength of composite beam as expected. When similar fiber contents are compared between STF and PPF, the fiber type has a negligible effect on the flexural strength (35SL25S vs 35SL20P or 10SF25S vs 10SF15P). Figure 17 shows that the predominant effect would be the strength of FR-SCC for repairing, but not the compatibility between Class A substrate and FR-SCC repairing material and compatibility strength is sufficient to resist the applied load.

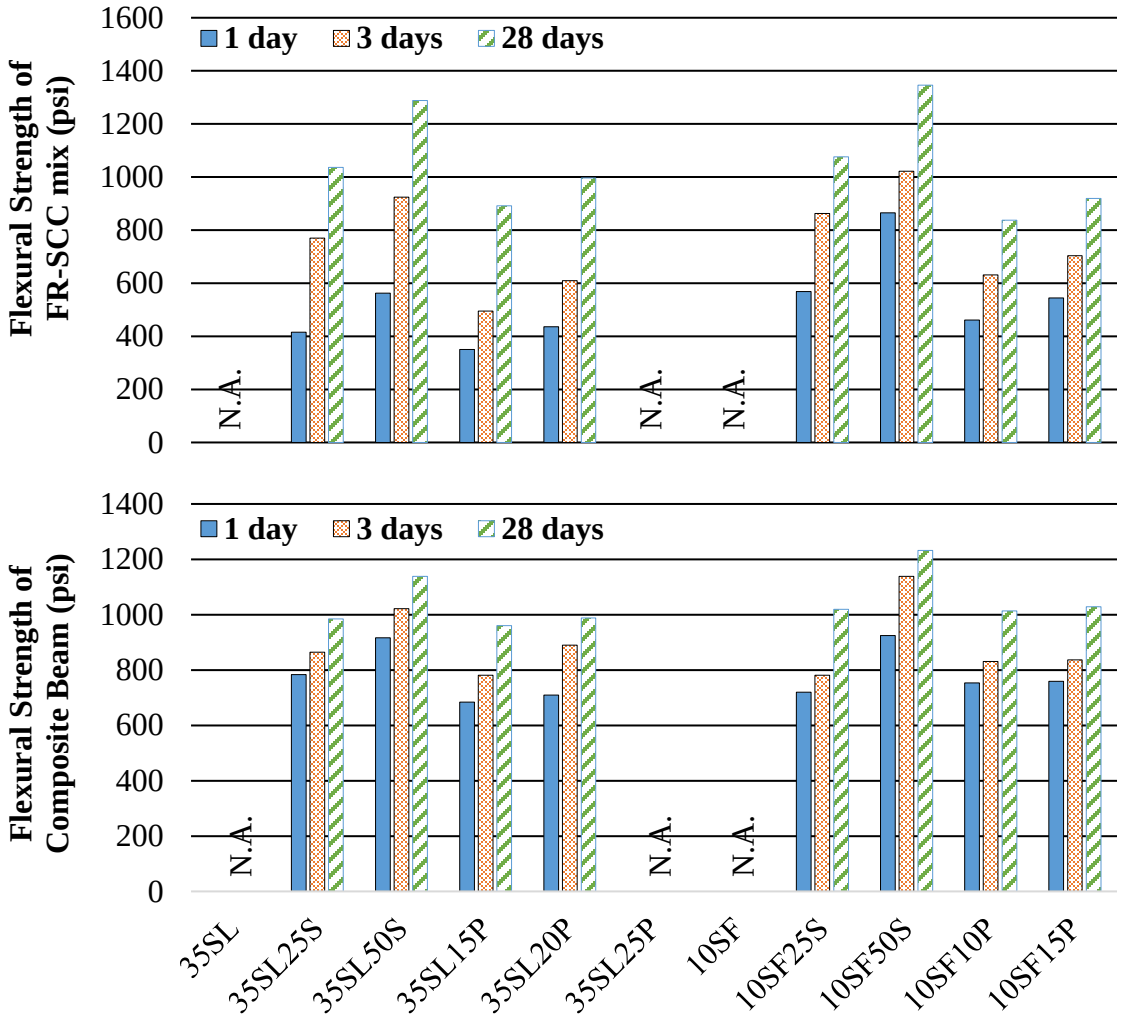

Figure 16 – Compatibility Testing Results

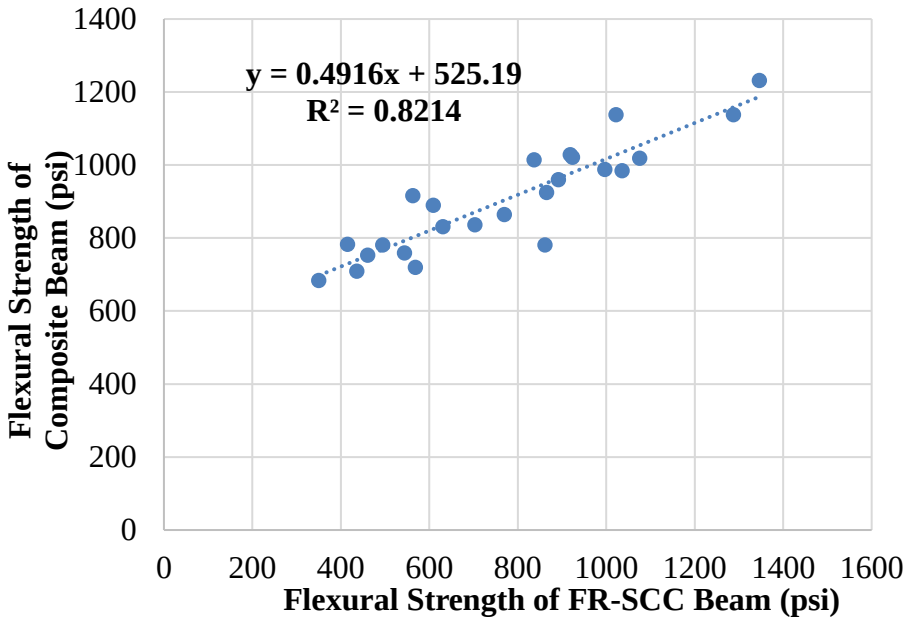

Figure 17 – Flexural Strength Correlation between FR-SCC and Composite

3.2.2 Bond Strength Test

Figure 18 summarizes the bond strength of composite slant cylinder. All cylinders were crashed at each end of the cylinder (substrate and FR-SCC repair material) which refers to good bond strength between two materials. The results show that the fiber content has a positive effect on the bond strength of composite cylinder, and higher fiber content resulted in improved bond strength.

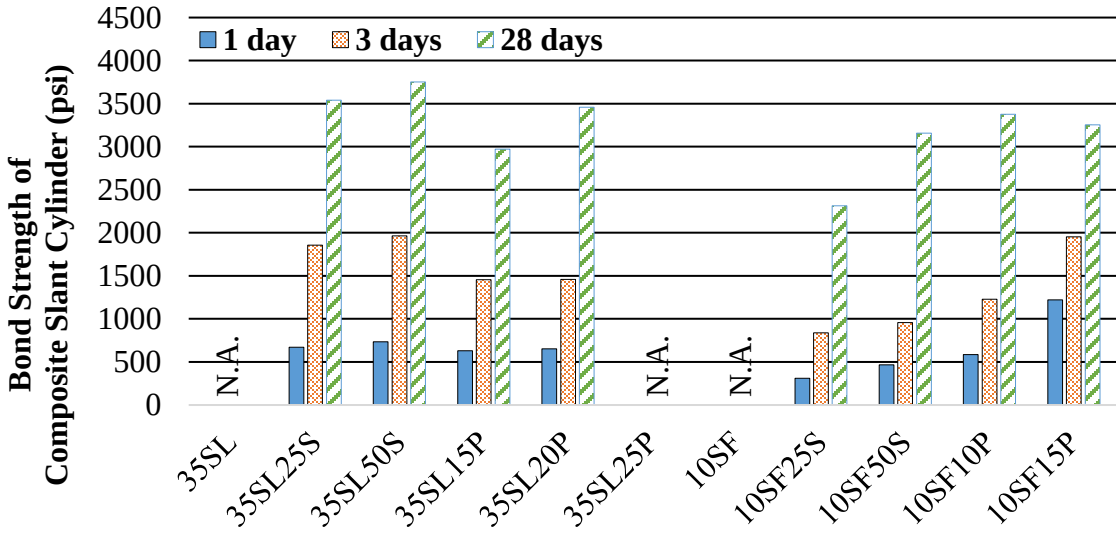

Figure 18 – Bond Strength Testing Results

3.3 Phase 3 Testing Results

3.3.1 Full-Scale Beam Testing

The load and deflection curves are plotted in Figure 19. A tri-linear load-deflection relationship was observed for both control beams and FR-SCC repaired beams. The first linear part of the curve represents the uncracked section which depends on the moment of inertia of each beam section. The moment of inertia is a property of the concrete cross-section, and therefore both beams (control and FR-SCC repair) show similar behavior. The second part is the post-cracking of the concrete up to steel yielding. A reduction in the beam stiffness was observed because the moment of inertia was reduced by cracking. The last part of the load-deflection curve represents the start of yielding of steel up to failure. The yielding of the steel reinforcement resulted in a dramatic degradation in the stiffness of the beam.

Table 6 summarizes the parameters and cracking/ultimate load of each beam tested. The flexural crack load ranges between 4.9 and 6.0 kips for the FR-SCC repaired beam, and 4.6 and 4.7 kips for the reference control beams. While the ultimate load ranges from 15.5 kips and 24.0 kips for the FR-SCC repaired beam, the reference control beams obtained 30.0 and 32.0 kips of ultimate load. The cracking loads are approx. 15% to 37% of the ultimate load for each beam. When the load was reached to the ultimate load, the reinforcing steel bars continued in irreversible prolongation up to ultimate load level. Depending on the tensile and bond strength of fiber, the fibers can help to resist the tensile cracking and arrest enlargement of the crack width. Figure 20 shows the pictures taken by digital microscopic camera for each PPF and STF at failure.

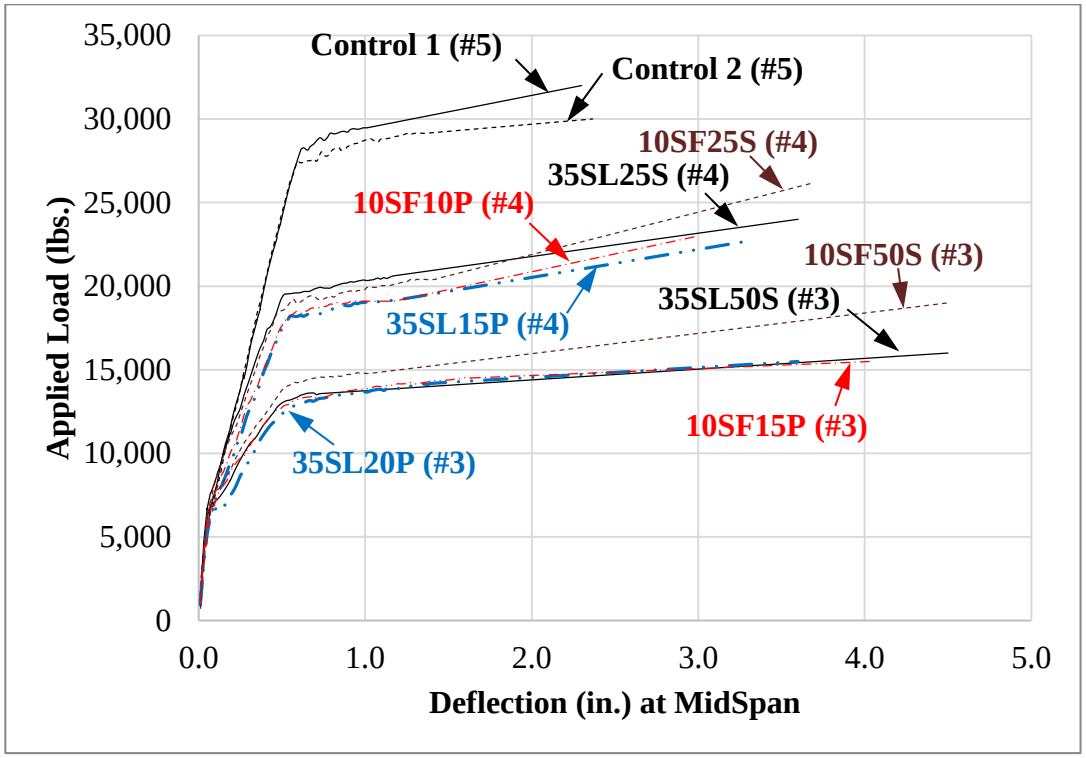

Figure 19 – Deflection at Midspan for Control Beams and FR-SCC Repaired Beams (see Sensor Location of L3 in Figure 12)

Table 6 – Cracking and Ultimate Load of Testing Beams

Specimen	SL (%wt.)	SF (%wt.)	STF (%vol.)	PPF (%vol.)	Rebar at FR-SCC Repair	Cracking Load, kips (Diff.*)	Ultimate Load, kips (Diff.*)
Control 1	-	-	-	-	**#5**	4.7	32.0
Control 2	-	-	-	-	**#5**	4.6	30.0
35SL25S	**35**	-	**0.25**	-	**#4**	5.5 (18.3%)	24.0 (-22.6%)
35SL50S	**35**	-	**0.50**	-	**#3**	5.7 (22.6%)	16.0 (-48.4%)
35SL15P	**35**	-	-	**0.15**	**#4**	4.9 (5.4%)	22.7 (-26.8%)
35SL20P	**35**	-	-	**0.20**	**#3**	5.1 (9.7%)	15.5 (-50%)
10SF25S	-	**10**	**0.25**	-	**#4**	5.5 (18.3%)	26.2 (-15.5%)
10SF50S	-	**10**	**0.50**	-	**#3**	6.0 (29%)	19.0 (-38.7%)
10SF10P	-	**10**	-	**0.10**	**#4**	5.5 (18.3%)	23.0 (-25.8%)
10SF15P	-	**10**	-	**0.15**	**#3**	5.7 (22.6%)	15.5 (-50%)

* Diff refers to the difference compared to the average load of two control beams.

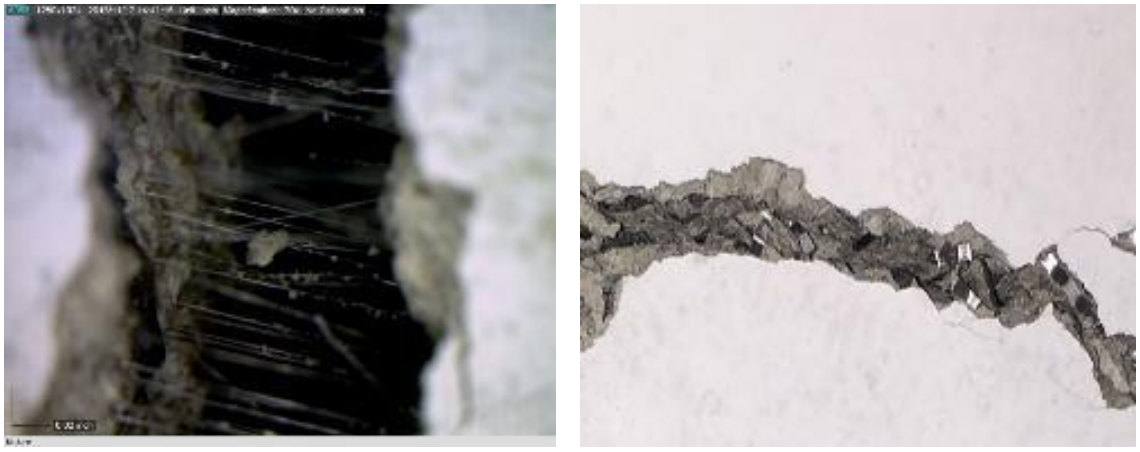

(a) (b)

Figure 20 – Crack at Failure; (a) PPE fiber, and (b) steel fiber

The percentage in parentheses in cracking load and ultimate load columns in Table 6 denotes the difference in applied load compared to the average of two control beams. The control beams have #5 rebars for longitudinal reinforcement, while the FR-SCC repaired beams have #3 or #4 rebars at the same location depending on the assumed rebar deterioration. The smaller diameter of bottom reinforcement represents the damaged rebar due to corrosion or deterioration. Smaller diameter of rebar was used for the FR-SCC mix with higher fiber content, and larger reinforcement was used for the FR-SCC mix with smaller fiber content. The FR-SCC repaired beam attained higher cracking load although these beams had smaller rebar dimeter. In addition, higher fiber content resulted in higher cracking capacity regardless of fiber types.

Figure 21 depicts how the fiber content affects the cracking load. It shows that the rebar size has no effect on the cracking load. When different fiber contents are compared, higher fiber volume provides better cracking resistance to the beams. However, it is not clear whether the fiber type

has any effect on the cracking load. This is because the initial cracking is dominant by the concrete strength and capacity (which is also affected by the fiber content), but not by the rebar capacity. Figure 22 represents the effect of rebar size on ultimate load. It is clear that the fiber content does not affect the ultimate capacity of the beam, but the rebar size has a remarkable effect on the ultimate load.

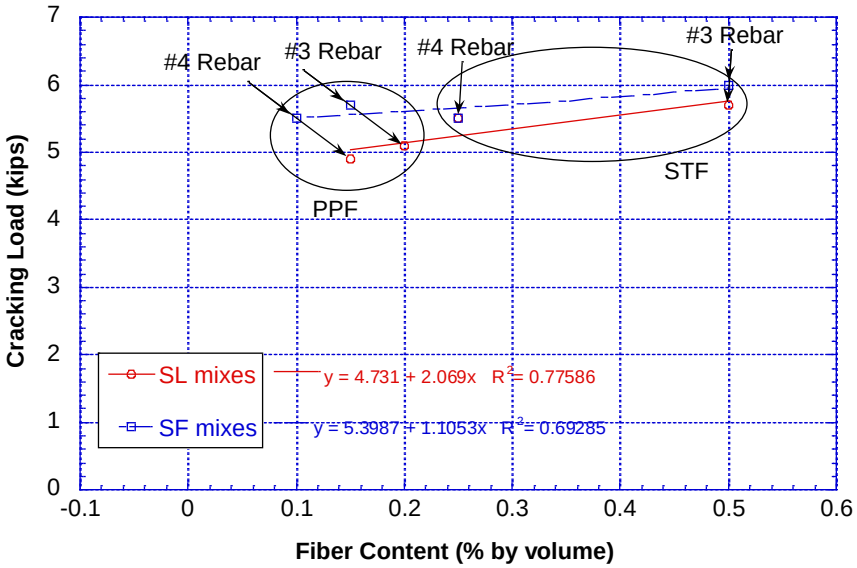

Figure 21 – Effect of Fiber Content on Cracking Load

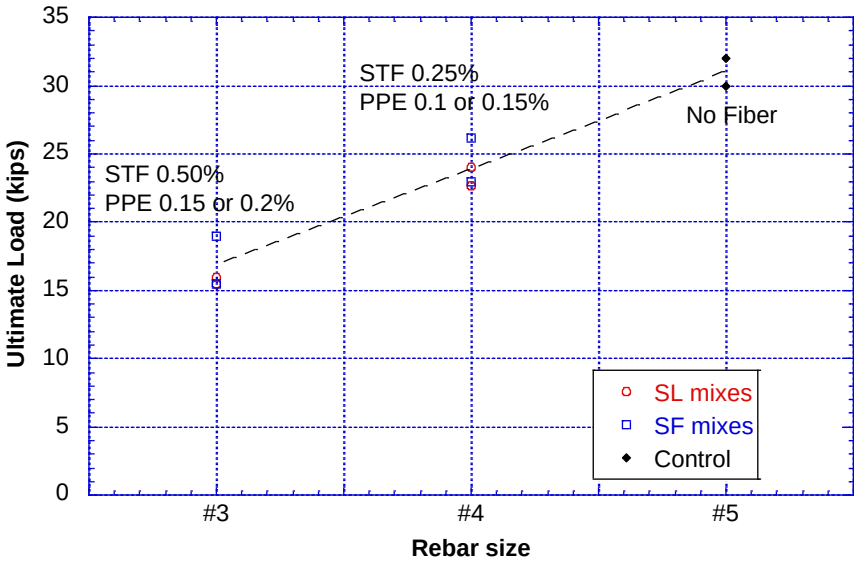

Figure 22 – Effect of Rebar Size on Ultimate Load

As a summary, SCC repaired beams attained 5.4% ~ 22.6% higher cracking load compared to the control beam because of the use of fibers and the fiber volume. However, the ultimate capacity of the FR-SCC repaired beam was reduced up to 50% compared to the control beam because of the smaller diameter of rebar.

The results show that the diameter of reinforcing rebars does not affect the initial cracking load, but does affect the ultimate load. In contrast, the amount of fiber (regardless of fiber type) affects the initial cracking capacity but does not affect the ultimate load. Therefore, the repair with FR-SCC could be an effective option to repair the damaged beam and to increase its cracking capacity. However, an additional effort should be made to recover the damaged reinforcement in order to maintain its original ultimate capacity.

Figure 23 shows the relationship between the applied load and the strain of the steel reinforcement at the mid span for control beams and FR-SCC repaired beams. The strain in the main steel reinforcement was measured by FSG at F3 as shown in Figure 12. The results show that after the main steel reinforcement exceeded its yield strain, it reached its hardening portion. The maximum service strains in the main steel reinforcement were 3500 and 3900 με for control and repaired beams, respectively. In general, the FR-SCC repaired beams with STF attained higher service strain than other beams with PPF. Such increase in the strain is mainly attributed by the higher flexural strength of concrete strengthened by the STF in the cement matrix.

Mode of failure of all beam specimens and their crack patterns are represented in Figure 24 and Figure 25, respectively.

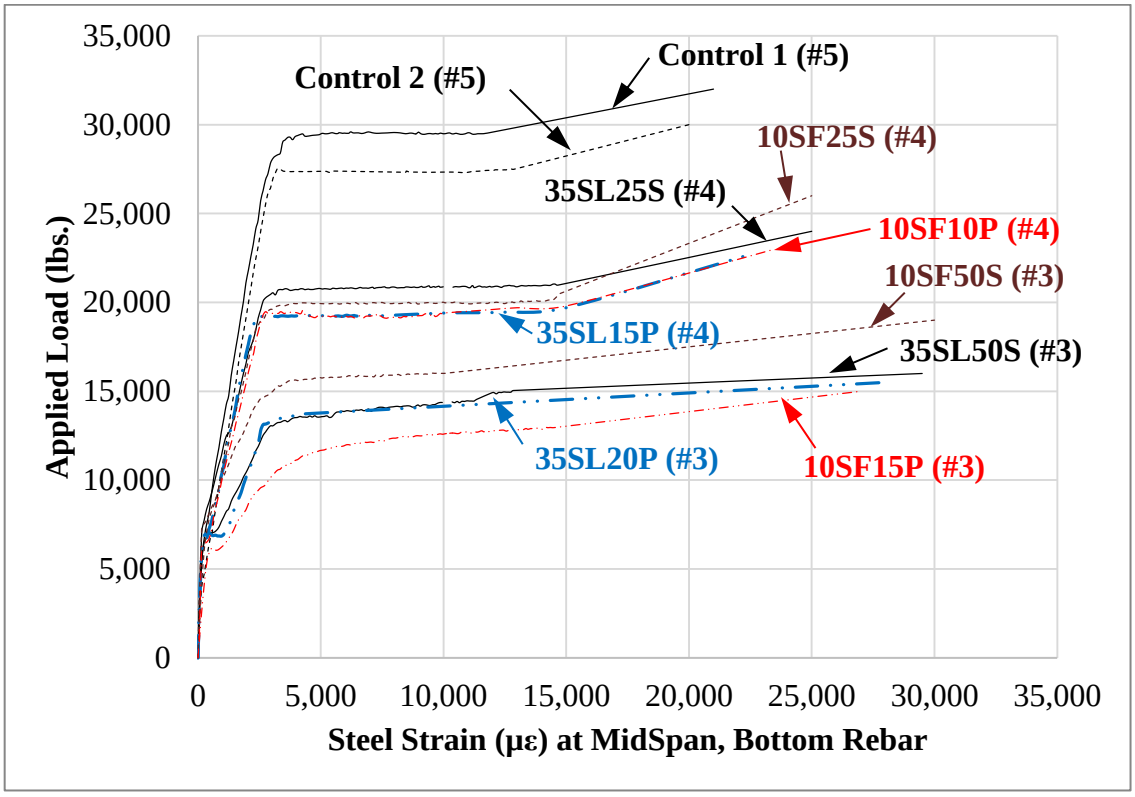

Figure 23 – Steel Strain at Midspan for Control Beams and FR-SCC Repaired Beams (see Sensor Location of F3 in Figure 12)

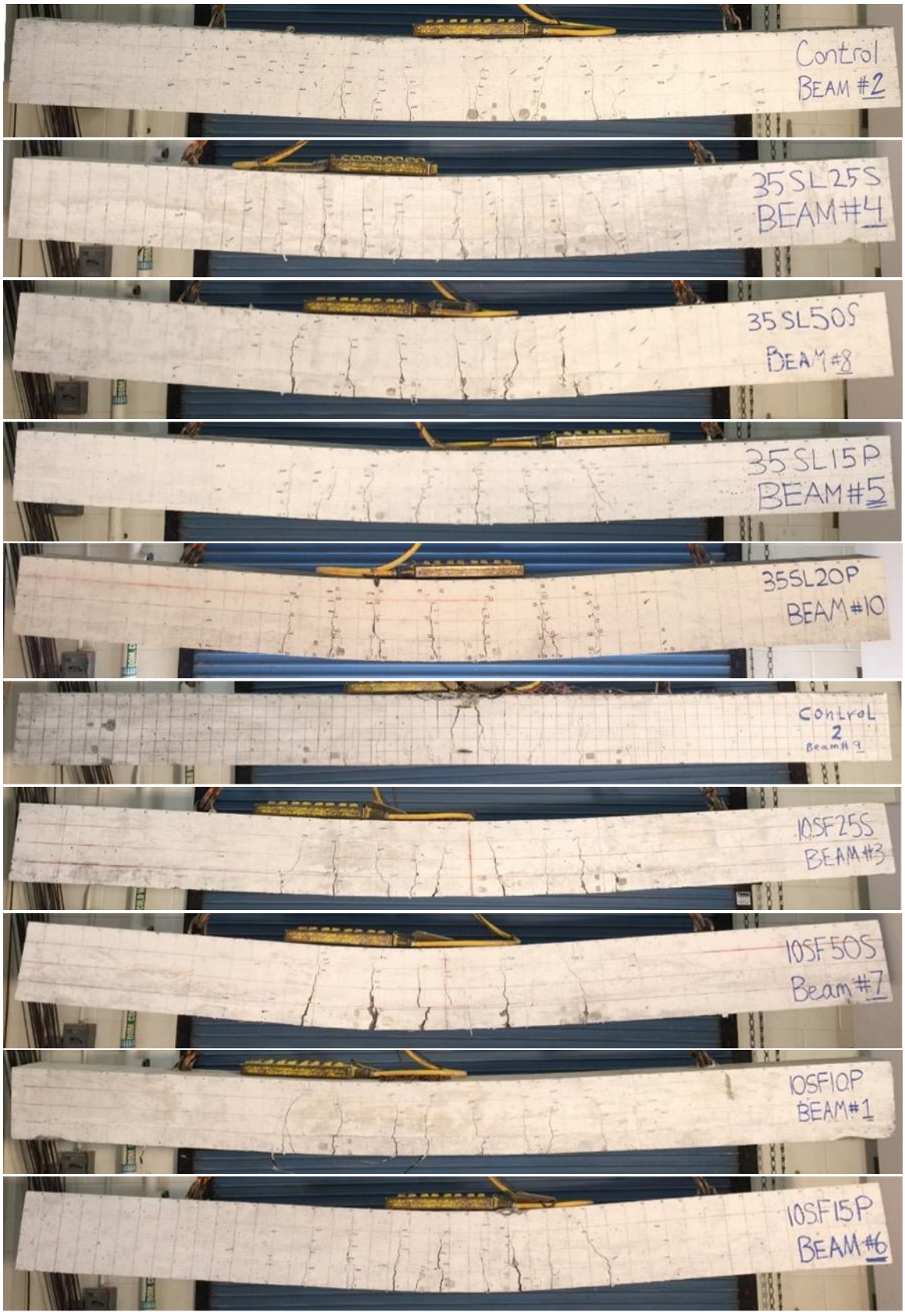
Control
BEAM #2
35SL25S
BEAM #4
35SL50S
BEAM #8
35SL15P
BEAM #5
35SL20P
BEAM #10
Control
2
Beam #9
10SF25S
BEAM #3
10SF50S
Beam #7
10SF10P
BEAM #1
10SF15P
BEAM #6

Figure 24 – Mode of Failure (Specimen name is written on the beam)

Control 1

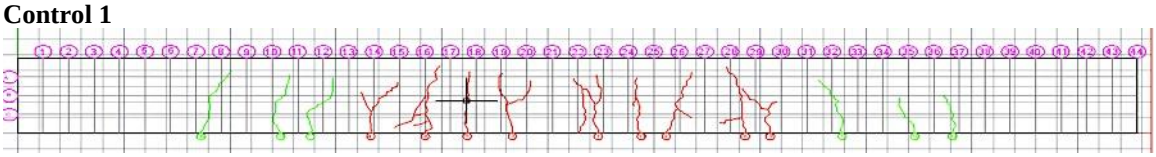

35SL25S

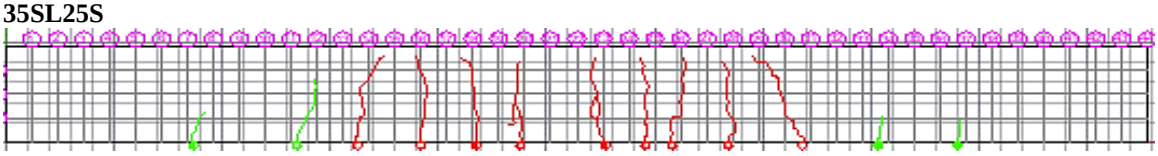

35SL50S

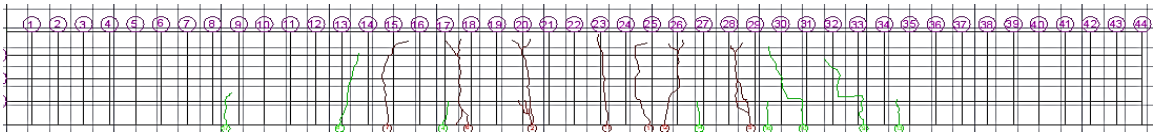

35SL15P

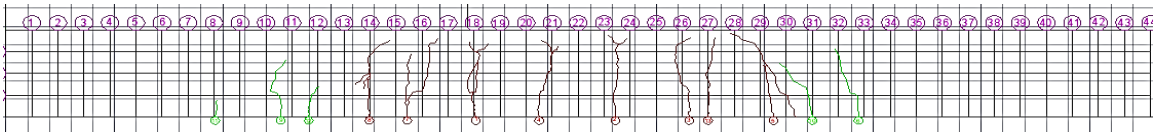

35SL20P

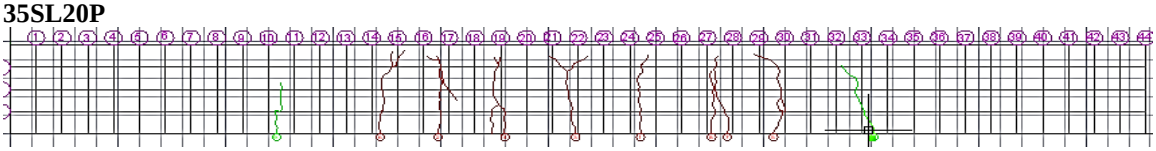

Control 2

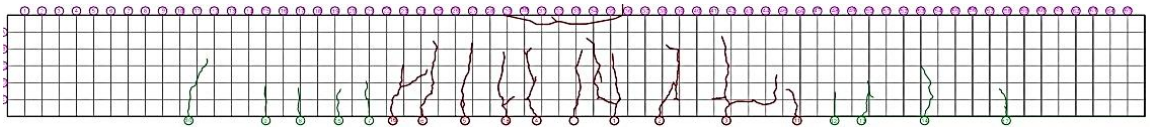

10SF25S

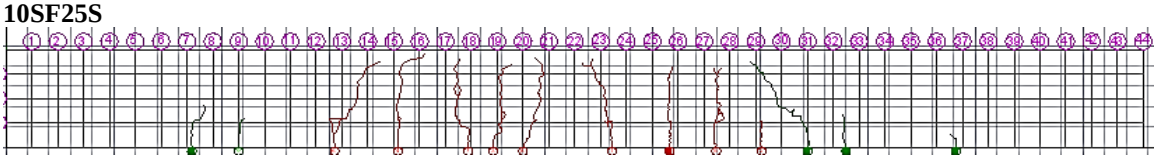

10SF50S

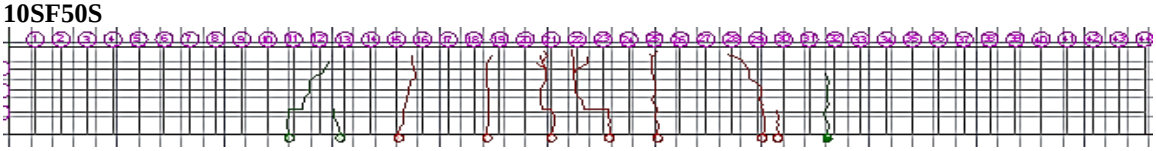

10SF10P

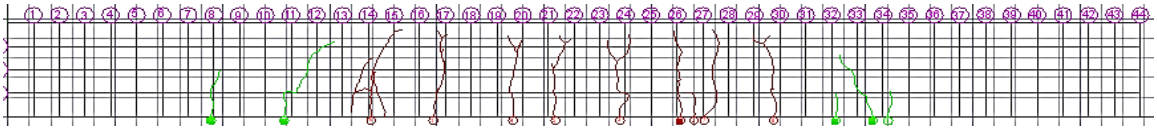

10SF15P

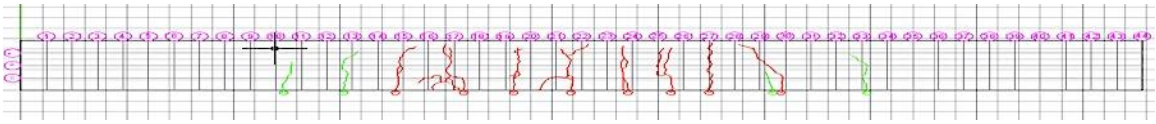

Figure 25 – Crack Patterns

4. Summary and Conclusions

Based on the experimental results of this study, the following conclusions can be made:

1) The PPF exhibited problems in the passing ability of the FR-SCC when the volume exceeds more than 0.2% by volume, and this effect is more dominant with SF mixes.

2) The SF mixes attained comparatively higher compressive strength than SL mixes. The maximum improvement in compressive strength was 71.7% for 10SF50S mix at 28 days compared to 10SF control mix.

3) The addition of STF increased the splitting tensile strength of concrete significantly. The splitting tensile strength of 10SF50S mix was 70.4 % higher than its reference 10SF mix.

4) The SF mixes attained higher flexural strength than the SL mixes. In general, the FR-SCC repair mixes showed higher flexural strength compared to Class A substrate mix at all ages.

5) The SL mixes showed lower shrinkage than the SF mixes because the SF particles are finer and therefore, are more reactive than SL particles. The incorporation of both fibers reduced the shrinkage significantly compared to the control mixes without fibers. The 35SL50S mix showed the lowest shrinkage which was 37 % lower than its reference 35SL mix at 56 days.

6) The failure location of compatibility test was the mid-point of the beam which indicates a good compatibility. The fiber type had a negligible effect on the flexural strength.

7) The STF is not as effective as PPF for bond strength. The mix with higher STF volume obtained similar bond strength as the mix with lower PPF volume.

8) The diameter of reinforcing rebars does not affect the initial cracking load but does affect the ultimate load. In contrast, the amount of fiber (regardless of fiber type) affects the initial cracking capacity but does not affect the ultimate load.

9) The repair with FR-SCC could be an effective and viable option to repair the damaged beam and to increase its cracking capacity. However, an additional effort should be made to recover the damaged reinforcement in order to maintain its original ultimate capacity.

References

1. Emmons, P. H. (2006). Vision 2020 Repair. *Protection Council, Strategic Development Council, American Concrete Institute's Concrete Research and Education Foundation (Jul. 1, 2006)* http://www.concretesdc.org/_pdfs/Vision2020-Version1.0_%20May2006.pdf
2. Goodwin, F. (2008). Renovation of the concrete repair industry. *Concrete Repair Bulletin, 21*(2), 12-17.
3. Kassimi, F., El-Sayed, A. K., & Khayat, K. H. (2014). Performance of Fiber-Reinforced Self-Consolidating Concrete for Repair of Reinforced Concrete Beams. ACI Structural Journal, 111(6).
4. Khayat, K.H., Aïtcin, P.-C. Use of Self-Consolidating Concrete in Canada - Present Situation and Perspectives, Proc., Workshop on Self-Compacting Concrete, JSCE Concrete Engineering Series 30, Kochi, Japan, Ed. Ozawa, K., Ouchi, M., August 1998, pp. 11-22.
5. Khayat, K.H., Hwang, S.-D., and Bonneau, O., Durability of SCC Used in Repair Applications, Presentation, ACI Spring Convention 2010.
6. Nawy, E. G. (Ed.). (2008). Concrete construction engineering handbook. CRC press.
7. Newman, J., and Choo, B. S. (Eds.). (2003). *Advanced concrete technology 1-4*. Butterworth-Heinemann.
8. Ozyildirim, C., Use of SCC for the Repair of Bridge Substructures, Presentation, ACI Spring Convention 2013.
9. Vandewalle, L. (2002). Design of steel fibre reinforced concrete using the sigma-w method: principles and applications. Materials and Structures,35 (249), 262-278.